A NEW GLOBAL MAP OF LIGHT PLAINS FROM THE LUNAR RECONNAISSANCE ORBITER CAMERA. H. M. Meyer[1], M. S. Robinson[1], B. W. Denevi[2], and A. K. Boyd[1], [1]School of Earth and Space Exploration, Arizona State University, Tempe, AZ 85281 USA (hmmeyer1@asu.edu), [2]Johns Hopkins University Applied Physics Laboratory, Laurel, MD 20723 USA.

Introduction: The origin of lunar light plains has long been debated, particularly since the return of Apollo 16 impact breccias [e.g., 1]. Conflicting relative age estimates and geologic context suggest all light plains are ejecta from the Orientale and Imbrium basins [1-3] or from many impact events [4-6], or even volcanic eruptions [7-8]. However, the presence of cryptomaria beneath light plains is well established [e.g., 9-10], and many previously identified light plains deposits have since been interpreted as impact melt, meaning that not all light plains are formed by the same mechanism. It is not clear how much of the light plains are the result of primary ejecta emplaced on pre-existing smooth surfaces, ponding of impact melt, or debris from secondaries. In order to distinguish between the various origins of light plains deposits both at the local and global scale, a consistent global map of light plains is required.

Previous maps that included light plains [8, 11-15] relied on Lunar Orbiter, Zond 7 and 8, Mariner 10, and Apollo images, but inconsistent resolution and illumination conditions made it difficult to identify and compare units at the global scale. Since commissioning, the Lunar Reconnaissance Orbiter Camera (LROC) [16] has captured images of the surface at ~100 m/pixel with the Wide Angle Camera (WAC), and the LROC team produced global mosaics with near-constant illumination and resolution. Here, we present a new global map of lunar light plains mapped from these new WAC mosaics (**Fig. 1**).

Data and Methods: Light plains were mapped based on criteria of Eggleton and Schaber [1] and Scott et al. [12] as implemented by Meyer et al. [17] (ArcGIS at a scale of 1:300,000). Two LROC WAC monochrome mosaics of opposite illumination directions were used to identify smooth and relatively flat to undulatory terrain with distinct margins. The standard deviation of slopes calculated from the WAC topography (GLD100) [18] over three different baselines (1000, 667, and 333 meters) were used to evaluate the roughness of mapped plains. Smooth plains included in our map were discriminated from mare deposits using the global mare shapefile [19].

Images from the LROC Narrow Angle Camera (NAC) [16] at a pixel scale of ~50 cm and from the Terrain Camera (TC) [20] at a pixel scale of ~10 m were used to identify stratigraphic relationships and to look for small-scale features to aid in the interpretation of origin. A Clementine FeO map [21] was used to identify compositional characteristics as well as delineate between externally emplaced and locally derived material where possible.

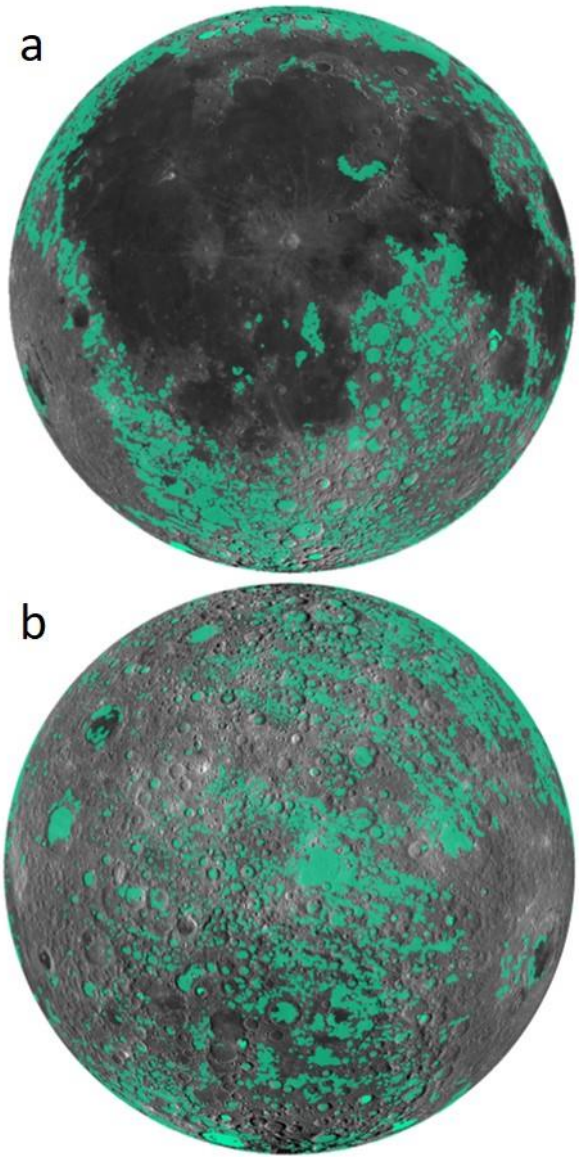

Fig. 1. Orthographic views of the (a) nearside (0°N 0°E) and (b) farside (2.7°S 168.7°W) light plains (green) overlain on the LROC WAC morphology basemap.

Observations: Light plains occupy ~9.5% of the surface: ~9 % of the farside and 10% of the nearside. Distinct ray-like clustering around the Orientale basin (**Fig. 1b**) suggests that the bulk of the farside light plains within 4 radii of the Orientale basin are related

to its formation, consistent with previous interpretations [17]. However, many farside light plains deposits likely originated with more regional to local impacts and pre-existing smooth surfaces (e.g., ancient impact melt, SPA mare deposits, or light plains). On the nearside (**Fig. 1a**), there is a cluster of light plains to the southeast of Orientale, many of which have been identified as Orientale ejecta overlying mare [10]. Mare flooding subsequent to the formation of Orientale obscures the surface to the east/northeast. Orientale formed on the boundary of the highlands and the low-lying nearside, so it is likely that pre-existing topography played a role in the distribution of deposits associated with the basin. Low-lying topography as well as pre-existing smooth surfaces may explain why the deposits to the southeast are more continuous and larger than those in the northwest, which are patchier and radial to the basin. There appears to be clustering around Imbrium as well, but, again, mare flooding has obscured much of the region that would be analogous to the region of clustered light plains outside Orientale. Light plains beyond ~2 radii from the western rim of Imbrium appear to be related to Orientale [17], suggesting extensive modification from the Orientale event largely erased any trend in light plains distribution associated with Imbrium in that region; a quantitative assessment is underway. Collectively, ~70% of all light plains may be related to the Imbrium and Orientale basins.

The South Pole-Aitken (SPA) basin is of particular interest because Orientale light plains affected a significant portion of the SPA terrain. Unlike the deposits to the northwest of Orientale, many of the light plains within SPA form large, continuous deposits and may be distinct in origin from the smaller, patchier deposits that cluster along radial paths from Orientale. Alternatively, pre-existing smooth surfaces could have allowed material mobilized by Orientale to spread laterally to form larger deposits. In the FeO map (**Fig. 2**), the light plains within SPA are distinctly enriched in FeO (red in Fig. 2) with respect to light plains outside SPA (yellow in Fig. 2), which is expected if the deposits are primarily derived from local material as suggested by [4].

Flow lobes were identified within many light plains deposits (e.g., **Fig. 3**) using Kaguya TC images and NAC images. These flows display a range of morphologies and sizes, and some are more heavily cratered than the terrain they embay. When compared with flows of known origins (e.g., impact melt or landslides), these smooth plains related flows may yield crucial insight into the physical properties and emplacement mechanisms of light plains.

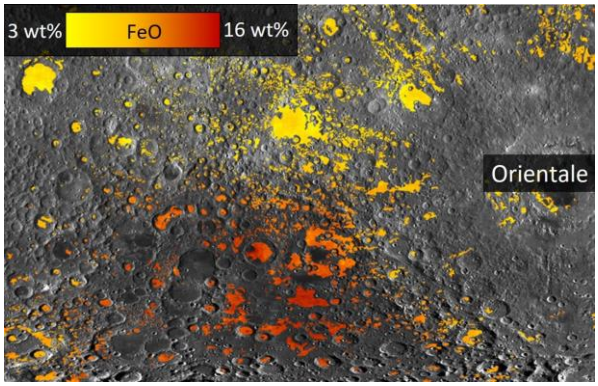

Fig. 2. FeO abundance for light plains deposits overlain on an LROC WAC mosaic.

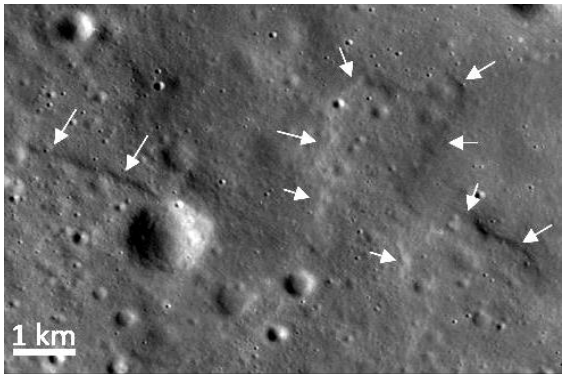

Fig. 3. Flow features within light plains ~1200 km from the rim of Orientale (29.616°N 249.588°E). White arrows denote flow margins. Kaguya TC Evening Mosaic v04.

References: [1] Eggleton R. E. and Schaber G. G. (1972), NASA Apollo 16 Prelim. Sci. Rep., 29-7–29-16., [2] Chao et al. (1973), Lunar Science IV, p127-128., [3] Howard et al. (1974), Rev. Geophys, Space Phys. 12(3), 309-327., [4] Oberbeck et al. (1974), LPSC 5, 111-136., [5] Oberbeck, V.R. et al. (1975), The Moon 12, 19–54., [6] Head (1974), The Moon 11(1-2), 77-99., [7] Milton, D.J. (1964), Astrogeol. Studies Ann. Prog. Rept., July 1963 to July 1964, pt. A, pp. 17–27., [8] Wilhelms and McCauley (1971), USGS I-703., [9] Schultz and Spudis (1979), LPSC 10, 2899-2918., [10] Whitten and Head (2015), Icarus, 247, 150-171., [11] Wilhelms and El-Baz (1977), USGS I-948., [12] Scott et al. (1977), USGS I-1034., [13] Stuart-Alexander (1978), USGS I-1047., [14] Lucchitta (1978), USGS I-1062., [15] Wilhelms, D.E. et al. (1979, USGS I-1162., [16] Robinson M. S. et al. (2010), Space Sci. Rev. 150, 81 -124., [17] Meyer et al. (2016), Icarus, 273, 135-145., [18] Scholten F. et al. (2011), JGR, 117, doi:10.1029/2011JE003926., [19] Nelson et al. (2014), LPSC 45, #2861., [20] Huruyama et al. (2008), EPS 60(4), 243-255., [21] Lucey, P. et al. (2000), JGR, 105(E8), 20297–20305.